HHS Public Access

Author manuscript

Sci Signal. Author manuscript; available in PMC 2024 May 14.

Published in final edited form as:

Sci Signal. 2023 November 14; 16(811): eadi3966. doi:10.1126/scisignal.adi3966.

Impaired intracellular Ca^{2+} signaling contributes to age-related cerebral small vessel disease in *Col4a1* mutant mice

Evan Yamasaki[1], **Pratish Thakore**[1], **Sher Ali**[1,⊕], **Alfredo Sanchez Solano**[1], **Xiaowei Wang**[2], **Xiao Gao**[3,4], **Cassandre Labelle-Dumais**[2], **Myriam M. Chaumeil**[3,4], **Douglas B. Gould**[2,5], **Scott Earley**[1,*]

[1]Department of Pharmacology, Center for Molecular and Cellular Signaling in the Cardiovascular System, University of Nevada, Reno School of Medicine, Reno, NV 89557-0318, USA

[2]Department of Ophthalmology, UCSF School of Medicine, San Francisco, CA 94158, USA

[3]Department of Physical Therapy and Rehabilitation Science, UCSF School of Medicine, San Francisco, CA 94143, USA

[4]Department of Radiology and Biomedical Imaging, UCSF School of Medicine, San Francisco, CA 94143, USA

[5]Department of Anatomy, Institute for Human Genetics, Cardiovascular Research Institute, Bakar Aging Research Institute, UCSF School of Medicine, San Francisco, CA 94158, USA

Abstract

Humans and mice with mutations in *COL4A1* and *COL4A2* manifest hallmarks of cerebral small vessel disease (cSVD). Mice with a missense mutation in *Col4a1* at amino acid 1344 (*Col4a1*$^{+/G1344D}$) exhibit age-dependent intracerebral hemorrhages (ICHs) and brain lesions. Here, we report that this pathology was associated with the loss of myogenic vasoconstriction, an intrinsic vascular response essential for the autoregulation of cerebral blood flow. Electrophysiological analyses showed that the loss of myogenic constriction resulted from blunted pressure-induced smooth muscle cell (SMC) membrane depolarization. Furthermore, we found that dysregulation of membrane potential was associated with impaired Ca^{2+}-dependent activation of large-conductance Ca^{2+}-activated K^+ (BK) and transient receptor potential melastatin 4 (TRPM4) cation channels linked to disruptions in sarcoplasmic reticulum (SR) Ca^{2+} signaling. *Col4a1* mutations impair protein folding, which can cause SR stress. Treating *Col4a1*$^{+/G1344D}$ mice with 4-phenylbutyrate, a compound that promotes the trafficking of misfolded proteins and alleviates SR stress, restored SR Ca^{2+} signaling, maintained BK and TRPM4 channel activity,

*Corresponding author: **Address Correspondence To**: Scott Earley, Ph.D., University of Nevada, Reno School of Medicine, Manville Health Sciences Building, Room 8, MS-0318, Reno, NV 89557-0318, USA, Phone: (775) 784-4117, Fax: (775) 784-1620, searley@med.unr.edu.

⊕Current position. Center for Translational Cancer Research, Institute of Biosciences and Technology, Texas A&M University, Houston, TX, 77030, United States of America

Author contributions: S.E. and D.B.G. initiated and supervised the project. S.E. designed the experiments. E.Y. performed brain histology, pressure myography, sharp electrode and patch-clamp electrophysiology, Ca^{2+} imaging, and ddPCR experiments. X.W. and X.G. performed magnetic resonance imaging experiments. S.A. and A.S.S. performed patch-clamp electrophysiology experiments. P.T. performed pressure myography experiments. C.L.D. performed animal colony management. E.Y., S.A., A.S.S., P.T., X.G., and S.E. analyzed the data. E.Y. and S.E. drafted the manuscript and prepared the figures. E.Y., C.L.D, M.M.C., D.B.G., and S.E. revised the manuscript.

Competing interests: The authors declare that they have no competing interests.

prevented loss of myogenic tone, and reduced ICHs. We conclude that alterations in SR Ca^{2+} handling that impair ion channel activity result in dysregulation of SMC membrane potential and loss of myogenic tone and contribute to age-related cSVD in *Col4a1*$^{+/G1344D}$ mice.

Introduction

Cerebral small vessel diseases (cSVDs) are a group of related pathologies that damage arteries, arterioles, venules, and capillaries in the brain. cSVDs are a substantial cause of stroke and, after Alzheimer's disease, are the second leading cause of cognitive impairment and dementia [1,2]. The underlying pathogenic mechanisms remain largely unknown, and no specific treatment options exist. Sporadic and familial forms of cSVD share clinical and radiological features, including white matter hyperintensities, dilated perivascular spaces, lacunar infarcts, microbleeds, and intracerebral hemorrhages (ICHs) [3–6]. Individuals with Gould syndrome, a rare multisystem disorder caused by autosomal dominant mutations in collagen IV alpha 1 (*COL4A1*) and alpha 2 (*COL4A2*), manifest these hallmarks [7–9]. The majority of pathogenic *COL4A1* and *COL4A2* mutations result in substitutions of critical glycine (Gly) residues with other amino acids within triple helical domains [10]. These mutations impair the formation and secretion of COL4A1 and COL4A2 heterotrimers [α1α1α2(IV)] leading to collagen [α1α1α2(IV)] deficiency in the basement membrane, and cause intracellular retention of misfolded mutant collagen that can lead to endoplasmic reticulum (ER) stress [11–13]. However, it is unclear how these defects lead to cSVD. *Col4a1* and *Col4a2* mutations demonstrate position-dependent effects contributing to phenotypic heterogeneity [13]. For the current study, we investigated the pathogenesis of *Col4a1*-associated cSVD using mice heterozygous for a missense mutation that changes the Gly residue at amino acid position 1344 to aspartate (Asp). These animals, designated *Col4a1*$^{+/G1344D}$, model the most common type of mutation in humans and develop severe cSVD pathology compared to other mutant mice carrying glycine missense mutations in a murine allelic series of *Col4a1* and *Col4a2* mutations [10,13].

Distinctive attributes of the cerebral vasculature serve the unique requirements of the brain. For example, cerebral arteries and arterioles exhibit graded constriction in response to changes in intravascular pressure. This vital autoregulatory process, known as the vascular myogenic response, protects downstream capillary beds from potentially harmful increases in perfusion pressure when cardiac output is transiently elevated during exercise or other stimuli [14]. The myogenic response is intrinsic to vascular smooth muscle cells (SMCs) and requires the coordinated activity of several ion channels. Increases in intraluminal pressure activate transient receptor potential melastatin 4 (TRPM4) channels, allowing an influx of Na^+ ions that depolarizes the plasma membrane to increase voltage-dependent Ca^{2+} inflow through Cav1.2 Ca^{2+} channels and engage the contractile apparatus [15,16]. Knockdown of TRPM4 in vivo decreases cerebral artery myogenic constriction and impairs cerebral blood flow autoregulation [17]. Pressure-induced membrane depolarization is balanced by hyperpolarizing currents conducted by several K^+-permeable ion channels, including large-conductance Ca^{2+}-activated K^+ (BK) channels, voltage-dependent K^+ (K_V) channels, and others [18–20]. The interplay of depolarizing and hyperpolarizing currents controls the resting membrane potential of SMCs and maintains cerebral arteries in a state of partial contraction.

BK and TRPM4 channels require high levels of intracellular Ca^{2+} for activation and, under native conditions, are stimulated by Ca^{2+} released from the sarcoplasmic reticulum (SR) through ryanodine receptors (RyRs) and inositol trisphosphate receptors (IP_3Rs), respectively [18,21]. Impairment of the myogenic response has been implicated in many types of cerebrovascular disease, including familial cSVDs associated with cerebral autosomal dominant arteriopathy with subcortical infarcts and leukoencephalopathy (CADASIL) caused by mutations in *NOTCH3* [22]. However, the impact of the *Col4a1*^{G1344D} mutation on the myogenic response is not known.

Here, we report that *Col4a1*$^{+/G1344D}$ mice exhibit age-dependent loss of myogenic tone that is associated with spontaneous ICHs and brain lesions detected by susceptibility-weighted magnetic resonance imaging (SWI). The deficit in myogenic tone resulted from diminished stretch-induced activation of TRPM4 channels and subsequent impairment of SMC membrane depolarization. We also found that subcellular and global Ca^{2+} signals generated by releasing Ca^{2+} from the SR through RyRs and IP_3Rs were disrupted in SMCs from aged *Col4a1*$^{+/G1344D}$ mice. Treating *Col4a1*$^{+/G1344D}$ mice with 4-phenylbutyrate (4PBA), a small molecule with chaperone properties that improves the secretion of misfolded proteins from the ER/SR [10,13,23–26], prevented SR Ca^{2+} signaling defects, preserved TRPM4 channel activity, attenuated the loss of myogenic tone, and largely prevented ICHs. These data provide evidence that impaired secretion of misfolded mutant α1α1α2(IV) collagen by SMCs from *Col4a1*$^{+/G1344D}$ mice causes disruptions in intracellular Ca^{2+} signaling, stretch-induced activation of TRPM4 channels, pressure-induced SMC membrane potential depolarization, and myogenic constriction. Our data also suggests these defects contributed to spontaneous age-related ICHs in *Col4a1*$^{+/G1344D}$ mice. Thus, the findings of this study reveal an age-dependent facet of cSVD pathogenesis.

Results

Col4a1$^{+/G1344D}$ mice exhibit age-dependent pathology.

All studies utilized *Col4a1*$^{+/G1344D}$ mice carrying a missense mutation at amino acid 1344 near the C-terminus of the triple helical domain (Fig. 1A) and *Col4a1*$^{+/+}$ littermates as controls. Age is the most critical risk factor for cSVD and vascular dementia [27,28]. To investigate age-related aspects of cSVD pathology, mice were studied at 3 and at least 12 months (M) of age, representing the young adult and middle age stages of life, respectively. Male and female mice were used throughout the study, and no sex-specific differences were detected.

Spontaneous ICHs is a highly penetrant and consequential manifestation of *Col4a1* mutations that increases in severity with age [10,29,30]. ICH severity was measured in brain sections from *Col4a1*$^{+/+}$ and *Col4a1*$^{+/G1344D}$ mice stained with Prussian blue. ICHs were not detected in 3 M-old *Col4a1*$^{+/+}$ mice. Low-level, punctate Prussian blue staining was present in brain sections from 3 M-old *Col4a1*$^{+/G1344D}$ mice (Fig. 1, B and C). 12 M-old *Col4a1*$^{+/+}$ mice did not exhibit ICHs, but brain sections from 12 M-old *Col4a1*$^{+/G1344D}$ mice displayed large areas of Prussian blue staining mainly localized to the subcortical regions (Fig. 1, D and E). The total area of Prussian blue staining in 12 M-old *Col4a1*$^{+/G1344D}$ mice

was nearly 20-fold greater than in 3 M-old mutants (1.9% compared to 0.1% of brain area, respectively), indicating that the severity of spontaneous ICHs increased with age.

Neuroimaging is frequently used to diagnose cSVD in human patients [31]. SWI showed 12 M-old *Col4a1*$^{+/+}$ mice did not exhibit SWI-detectable brain lesions, but brains from age-matched *Col4a1*$^{+/G1344D}$ mice had multiple lesions, mainly localized to the thalamus (Fig. 1, F to I). The number, total volume, and localization of brain lesions detected with SWI were consistent with ICHs detected with Prussian blue staining.

Diminished pressure-induced constriction of cerebral arteries from 12 M-old *Col4a1*$^{+/G1344D}$ mice is due to impaired SMC membrane depolarization.

To better understand the underlying causes of ICHs in *Col4a1*$^{+/G1344D}$ mice, we used ex vivo pressure myography to study the myogenic response of cerebral arteries [32]. Vasoconstriction in response to stepwise increases in intraluminal pressure (from 5 to 120 mmHg) was evaluated by measuring the active steady-state and passive luminal diameter of cannulated cerebral arteries bathed in standard physiological saline solution at each pressure and calculating myogenic tone. The myogenic tone of cerebral arteries isolated from 3 M-old *Col4a1*$^{+/+}$ and *Col4a1*$^{+/G1344D}$ mice did not differ (Fig. 2, A and B). However, cerebral arteries from 12 M-old *Col4a1*$^{+/G1344D}$ mice barely constricted in response to pressure and had significantly lower levels of myogenic tone than those from age-matched *Col4a1*$^{+/+}$ mice (Fig. 2, C and D). The passive diameters of cerebral arteries isolated from 12 M-old *Col4a1*$^{+/+}$ and *Col4a1*$^{+/G1344D}$ mice did not differ (fig. S1), suggesting that changes in myogenic tone were not due to alterations in the mechanical properties of the vessel wall.

Increases in intraluminal pressure cause SMCs in the vascular wall to depolarize [33], triggering voltage-dependent Ca^{2+} influx and muscular contraction [33,34]. To determine if the loss of myogenic tone in 12 M-old *Col4a1*$^{+/G1344D}$ mice was associated with impaired pressure-induced depolarization, we recorded the membrane potentials of SMCs in intact cerebral arteries using intracellular microelectrodes. At low intraluminal pressure (20 mmHg), the membrane potential of SMCs in cerebral arteries from 3 M-old *Col4a1*$^{+/+}$ and *Col4a1*$^{+/G1344D}$ mice did not differ (Fig. 2, E and F). Increasing intraluminal pressure to physiological levels (80 mmHg) depolarized the SMC membrane potential in arteries from both groups to the same extent (Fig. 2, E and F). SMC membrane potential did not differ between vessels from 12-M old *Col4a1*$^{+/+}$ or *Col4a1*$^{+/G1344D}$ animals when arteries were pressurized to 20 mmHg, but when intraluminal pressure was increased to 80 mmHg, the depolarization of SMCs in cerebral arteries from *Col4a1*$^{+/G1344D}$ mice was significantly blunted compared with controls (Fig. 2, G and H). These data suggest that cerebral arteries from 12 M-old *Col4a1*$^{+/G1344D}$ mice lose myogenic tone because pressure-induced SMC membrane depolarization is impaired.

Age-dependent declines in BK and TRPM4 channel activity in SMCs from *Col4a1*$^{+/G1344D}$ mice.

To determine if changes in ion channel activity account for impaired pressure-induced SMC depolarization, we used patch-clamp electrophysiology to compare hyperpolarizing K_V and BK currents and depolarizing TRPM4 currents in native SMCs from control

and *Col4a1*$^{+/G1344D}$ mice. Elevated SMC K_V channel current density is responsible for diminished myogenic tone in cerebral arteries from CADASIL cSVD mice [22]. We measured K_V currents in freshly isolated SMCs to determine if a similar mechanism accounts for the loss of myogenic tone in cerebral arteries from 12 M-old *Col4a1*$^{+/G1344D}$ mice. K_V currents were recorded in the perforated patch-clamp configuration to maintain the integrity of intracellular signaling cascades. Whole-cell currents were evoked by applying voltage steps from a holding potential of −80 mV in the presence of selective BK channel blocker paxilline, then in the presence of K_V channel blocker 4-aminopyridine. K_V current amplitude was determined at each potential by subtraction. We found that K_V current amplitudes did not differ between SMCs from 12 M-old *Col4a1*$^{+/+}$ and *Col4a1*$^{+/G1344D}$ mice at all applied command potentials (fig. S2, A and B).

The activity of BK channels in cerebral artery SMCs under native conditions is driven by the transient release of Ca^{2+} ions through RyRs on the SR into restricted subcellular microdomains proximal to the plasma membrane [35]. These signaling events, known as Ca^{2+} sparks, activate clusters of BK channels on the plasma membrane to generate large-amplitude spontaneous transient outward currents (STOCs) [18,19]. We utilized the perforated patch-clamp configuration to measure STOCs in cerebral artery SMCs from 3 M-old *Col4a1*$^{+/+}$ and *Col4a1*$^{+/G1344D}$ mice over a range of command potentials (−60 to 0 mV) and saw no significant difference in STOC frequency or amplitude (Fig. 3, A to C). However, the frequency and amplitude of STOCs were significantly lower in cerebral artery SMCs from 12 M-old *Col4a1*$^{+/G1344D}$ mice compared with age-matched controls (Fig. 3, D to F). To determine if decreases in STOCs resulted from changes in the amount of functional BK channels at the plasma membrane, we utilized the conventional whole-cell patch clamp configuration to measure K^+ currents during voltage-clamp steps from a holding potential of −80 mV. The BK-dependent component of the current was isolated with paxilline. We found that BK current amplitudes did not differ between SMCs from 12 M-old *Col4a1*$^{+/+}$ and *Col4a1*$^{+/G1344D}$ mice at all applied command potentials (fig. S3, A and B). We also assessed gene expression by ddPCR to measure transcript levels of *Kcnma1* (which encodes the BK α subunit), *Kcnmb1* (which encodes the BK β1 subunit), and *Ryr2* (which encodes ryanodine receptor 2). No differences in mRNA expression levels were detected (fig S4). Because reduced BK channel activity depolarizes SMC membrane potential and increases contractility [36], diminished BK channel activity in SMCs from 12 M-old *Col4a1*$^{+/G1344D}$ mice cannot account for impaired pressure-induced membrane depolarization.

TRPM4 is a Ca^{2+}-activated, nonselective monovalent cation channel required for pressure-induced SMC depolarization and the development of myogenic tone in cerebral arteries [15,16,37,38]. At the membrane potentials of SMCs in the vascular wall under physiological conditions (−60 to −30 mV), TRPM4 channels conduct inward Na^+ currents that depolarize the plasma membrane in response to increases in intraluminal pressure [15,39]. Impaired TRPM4 channel activity is responsible for loss of myogenic tone in a mouse model of Gould syndrome caused by a *Col4a1*^{G394V} mutation [30]. Therefore, patch-clamp electrophysiology was used to determine if TRPM4 activity was diminished in *Col4a1*$^{+/G1344D}$ mice. We assessed channel function and availability in freshly isolated cerebral artery SMCs using the conventional whole-cell patch-clamp configuration with a high [Ca^{2+}] intracellular solution to directly activate TRPM4. Currents were recorded as voltage ramps were applied in the

absence or presence of theTRPM4 blocker 9-phenanthrol[15], and TRPM4 currents were isolated by subtraction. Prior studies using ion substitution protocols have shown that Ca^{2+}-activated, 9-phenanthrol currents recorded using these methods are carried by Na^+ ions, providing substantial evidence that these are bona fide TRPM4 currents [16,37,40]. We found that the amplitudes of whole-cell TRPM4 currents recorded from cerebral artery SMCs did not differ between *Col4a1*$^{+/+}$ and *Col4a1*$^{+/G1344D}$ mice at 3 and 12 M of age (Fig. 3, G to J). These data indicate that the collagen mutation studied here does not directly affect TRPM4 channel function or the trafficking of channel protein to the plasma membrane.

TRPM4 channels in SMCs are activated by a signal transduction cascade initiated by angiotensin II type 1 receptors (AT1Rs) [41–44]. Activation of $G\alpha_q$ protein-coupled AT1Rs stimulates phospholipase C (PLC), leading to the cleavage of phosphatidylinositol 4,5-bisphosphate (PIP_2) into diacylglycerol and inositol triphosphate (IP_3). IP_3 stimulates Ca^{2+} release from the SR through IP_3Rs to transiently activate TRPM4 channels [21,38,41]. AT1Rs are directly activated by the stretch of the plasma membrane (independently of their ligand) and are a critical mechanosensor in SMCs [41–44]. To measure the activity of TRPM4 channels in response to mechanical force, we patch-clamped SMCs in the perforated patch configuration and applied negative pressure (−20 mmHg) through the patch pipet to stretch the plasma membrane. Stretch-induced transient inward cation currents (TICCs) evoked in this manner are blocked by 9-phenanthrol or TRPM4 knockdown [15,21]. Stretch-activated TICC activity in SMCs from 3 M-old *Col4a1*$^{+/+}$ and *Col4a1*$^{+/G1344D}$ (Fig. 3, K and L) did not differ. In contrast, stretch-induced TICC activity in SMCs from 12 M-old *Col4a1*$^{+/G1344D}$ mice was significantly lower than that of age-matched *Col4a1*$^{+/+}$ mice (Fig. 3, M and N). To determine if altered gene expression underlies the reduction in TICC activity, we utilized ddPCR to measure transcript levels of *Trpm4* (which encodes TRPM4), *Itpr1* (which encodes IP_3R1), and *Itpr2* (which encodes IP_3R2) in cerebral arteries from 12 M-old *Col4a1*$^{+/+}$ and *Col4a1*$^{+/G1344D}$ mice. No differences in mRNA copy numbers were observed (fig. S4). These data suggest that blunted pressure-induced SMC depolarization and impaired myogenic tone result from diminished stretch-induced activation of TRPM4 channels.

Defective intracellular Ca^{2+} signaling in cerebral artery SMCs from 12 M-old *Col4a1*$^{+/G1344D}$ mice.

Ca^{2+} released from the SR drives BK and TRPM4 channel activity in cerebral artery SMCs [18,21]. Therefore, we investigated the possibility that these vital Ca^{2+} signaling pathways are disrupted in SMCs from 12 M-old *Col4a1*$^{+/G1344D}$ mice. High-speed, high-resolution spinning disk confocal microscopy imaging of freshly isolated SMCs loaded with the Ca^{2+}-sensitive fluorophore Fluo-4 AM detected spontaneous Ca^{2+} sparks in SMCs isolated from 3 M-old *Col4a1*$^{+/+}$ and *Col4a1*$^{+/G1344D}$ mice. The frequency, amplitude, duration, rise time, and decay rate did not differ between groups (Fig. 4, A to C). Spontaneous Ca^{2+} sparks were also present in SMCs isolated from both groups of 12 M-old mice. No significant differences in Ca^{2+} spark amplitude, duration, rise time, and decay rate were observed, but Ca^{2+} spark frequency was significantly lower in SMCs from 12 M-old *Col4a1*$^{+/G1344D}$ mice (Fig. 4, D to F). Thus, diminished Ca^{2+} spark frequency likely accounts for decreased STOC frequency in SMCs from 12 M-old *Col4a1* mutant mice.

Fluo-4 AM-loaded SMCs were challenged with the RyR agonist caffeine to investigate how RyR function was affected by the *Col4a1*^{G1344D} mutation [45]. Ca^{2+} signals arising from intracellular release were isolated from Ca^{2+} influx events by acutely removing Ca^{2+} from the extracellular solution immediately before recording. Caffeine-evoked global cytosolic [Ca^{2+}] increases did not differ between SMCs from 3 M-old *Col4a1*$^{+/+}$ and *Col4a1*$^{+/G1344D}$ mice (Fig. 4, G and H). In contrast, caffeine-induced global Ca^{2+} signals were smaller in amplitude in SMCs from 12 M-old *Col4a1*$^{+/G1344D}$ mice than in controls (Fig. 4, I and J). These data indicate that the release of SR Ca^{2+} from RyRs is impaired in the SMCs of *Col4a1*$^{+/G1344D}$ mice in an age-dependent manner.

Fluo-4 AM loaded-SMCs were also treated with the $G\alpha_q$ protein-coupled thromboxane A2 receptor agonist U46619 to investigate IP_3R-mediated Ca^{2+} signaling. U46619-induced Ca^{2+} signals did not differ between cerebral artery SMCs from 3 M-old *Col4a1*$^{+/+}$ and *Col4a1*$^{+/G1344D}$ mice (Fig. 4, K and L). In contrast, Ca^{2+} signals induced by U46619 were smaller in amplitude in SMCs from 12 M-old *Col4a1*$^{+/G1344D}$ mice compared to controls (Fig. 4, M and N). These data suggest that the release of SR Ca^{2+} from IP_3Rs is also impaired in the SMCs of *Col4a1*$^{+/G1344D}$ mice in an age-dependent manner.

RyRs and IP_3Rs share a common SR Ca^{2+} pool [46]. Impairment of Ca^{2+} release through both receptors suggests that the SR [Ca^{2+}] of SMCs from 12 M-old *Col4a1*$^{+/G1344D}$ mice is lower than that of corresponding controls. Further, diminished SR Ca^{2+} levels likely account for decreased Ca^{2+} spark frequency and diminished STOC and TICC activity.

4PBA prevents age-related cerebral artery defects in *Col4a1*$^{+/G1344D}$ mice.

Col4a1 mutations impair collagen α1α1α2(IV) secretion in vitro and in vivo, which can be alleviated by treatment with 4PBA [10,13,26,47]. The chemical chaperone 4PBA facilitates the trafficking of misfolded mutant proteins and reduces ER/SR stress [48]. To investigate a potential link between impaired collagen secretion and the cerebral vascular pathology of *Col4a1*$^{+/G1344D}$ mice, 4PBA was added to the drinking water of mutant and control animals from birth (postnatal day 0).

We found that 4PBA treatment prevented the diminishment of Ca^{2+} signals evoked by caffeine (Fig. 5, A and B) or U46619 (Fig. 5, C and D) in cerebral artery SMCs from 12 M-old *Col4a1*$^{+/G1344D}$ mice. 4PBA treatment also prevented age-dependent declines in Ca^{2+} spark frequency (fig. S5, A to C). We also found that 4PBA treatment averted the loss of STOC (fig. S5, D to F) and TICC (Fig. 5, E and F) activity. These data demonstrate that age-related defects in intracellular Ca^{2+} signaling that control ion channel activity and membrane potential were prevented by treating *Col4a1*$^{+/G1344D}$ mice with 4PBA. 4PBA treatment also prevented loss of myogenic tone (Fig. 5, G and H) and significantly diminished spontaneous ICHs in 12 M-old *Col4a1*$^{+/G1344D}$ mice (Fig. 5, I and J). These data suggest that 4PBA protects against age-dependent defects in myogenic tone and ICHs in *Col4a1*$^{+/G1344D}$ mice.

Discussion

Despite the devastating consequences of the disease, the molecular pathogenesis of cSVD is essentially unknown. Here we utilized the *Col4a1*$^{+/G1344D}$ mouse model of Gould syndrome

to investigate how this monogenic form of cSVD damages small arteries in the brain during aging. Our findings showed that these mice exhibited pathological changes with age, including the loss of myogenic tone, high levels of spontaneous ICHs, and brain lesions. Electrophysiology experiments revealed that the loss of myogenic tone was associated with diminished pressure-induced SMC depolarization and decreased activities of BK and TRPM4 channels. In addition, we found that fundamental RyR- and IP_3R-dependent Ca^{2+} signaling pathways were disrupted in SMCs from 12 M-old *Col4a1*$^{+/G1344D}$ mice, likely due to a reduction in SR Ca^{2+} levels. Treating *Col4a1*$^{+/G1344D}$ mice with the chemical chaperone 4PBA negated Ca^{2+} signaling disruptions, increased BK and TRPM4 channel activity, prevented loss of myogenic tone, and reduced spontaneous ICHs. We conclude that the age-dependent cSVD pathogenesis of *Col4a1*$^{+/G1344D}$ mice results from defects in SMC SR function that lead to reduced Ca^{2+} store load and disrupted intracellular Ca^{2+} signaling. Defects in subcellular Ca^{2+} signals diminish BK and TRPM4 channel activity, disrupting membrane potential regulation and impeding pressure-induced constriction of cerebral arteries. These findings reveal a mechanism that contributes to age-dependent cSVD (Fig. 6).

Myogenic constriction protects delicate capillaries in the brain from pressure overload during increases in cardiac output and perfusion associated with exercise, stress, and other stimuli [14]. Intracerebral hemorrhages in 12 M-old *Col4a1*$^{+/G1344D}$ mice were predominantly localized to the thalamus. This may be due to the proximity of the arteries that supply the thalamus to the Circle of Willis. The paramedian thalamic and tuberothalamic arteries branch directly off the Circle of Willis and the thalamogeniculate and posterior choroidal arteries branch off the posterior cerebral arteries proximal to the Circle of Willis [49]. The short distance from large arteries that carry higher pressures could account for the increased risk of intracerebral hemorrhage in the thalamus. The myogenic response is deficient in several monogenetic forms of cSVD [22,30,50]. However, the defects responsible for the loss of myogenic tone differ between disease models. For example, Dabertrand *et al.* linked the loss of myogenic tone in the CADASIL model with blunted pressure-induced SMC membrane potential depolarization and connected the defect in membrane potential regulation with increased surface expression of K_V channels and elevated hyperpolarizing K^+ current density [22]. Notably, depletion of the minor membrane phospholipid PIP_2, leading to the loss of TRPM4 channel activity, is the fundamental defect responsible for the loss of myogenic constriction in a mouse model of Gould syndrome caused by a *Col4a1*^{G394V} mutation [30]. Although both *Col4a1*^{G394V} and *Col4a1*^{G1344D} mutations cause TRPM4-related cerebrovascular dysfunction, there is no evidence of decreased PIP_2 levels in *Col4a1*$^{+/G1344D}$ mice. The current study uncovered a distinctive flaw in the SMCs of *Col4a1*$^{+/G1344D}$ cSVD mice – impaired Ca^{2+} signaling. Our data showed that the release of Ca^{2+} from the SR through RyRs and IP_3Rs became faulty in *Col4a1*$^{+/G1344D}$ mice by 12 M of age. Impaired SR Ca^{2+} release disrupted the activity of BK and TRPM4 channels. These channels play opposing roles in regulating SMC membrane potential and contractility. TRPM4 channels depolarize the membrane and promote contractility, whereas BK channels provide negative feedback to limit the magnitude of this response [51]. When pressure-induced membrane depolarization is impaired, the BK pathway is disengaged and has minimal influence on membrane potential [52].

Diminished levels of Ca^{2+} in the SR likely cause Ca^{2+} signaling and ion channel defects in SMCs from 12 M-old *Col4a1*$^{+/G1344D}$ mice. This concept is supported by prior studies showing that a ~16% decrease in SR [Ca^{2+}] diminished STOC frequency by 70% and that a >20% decrease in SR [Ca^{2+}] completely abolished IP_3R-mediated Ca^{2+} release in native SMCs [53,54]. In many types of cells, store-operated Ca^{2+} entry (SOCE) protects against decreases in ER/SR [Ca^{2+}] [55]. However, SOCE is virtually undetectable in native, contractile vascular SMCs, thereby enhancing their susceptibility to pathogenic SR Ca^{2+} depletion [52,56,57]. We conclude that SR Ca^{2+} store depletion and the resulting dysregulation of BK, TRPM4, and SMC membrane potential is responsible for the age-related loss of myogenic tone in *Col4a1*$^{+/G1344D}$ cSVD mice.

Steady-state free Ca^{2+} levels in the ER/SR are maintained by the release of Ca^{2+} into the cytosol through RyRs and IP_3Rs, mobile and stationary Ca^{2+}-binding proteins in the SR lumen, and transport of Ca^{2+} from the cytosol into the SR by sarco/endoplasmic reticulum ATPase (SERCA) enzymes [46]. Disruption of one or more of these elements could lead to SR Ca^{2+} defects in *Col4a1*$^{+/G1344D}$ mice. These mice display impaired secretion and increased intracellular accumulation of collagen α1α1α2(IV), presumably due to difficulties associated with the trafficking of misfolding of mutant proteins out of the ER/SR [10,13]. Misfolded proteins can cause ER/SR stress [58] that is associated with the depletion of Ca^{2+} stores [59]. For example, Yamato *et al.* [60] demonstrated that tunicamycin-induced ER stress promotes RyR-mediated Ca^{2+} leak, potentially due to increased reactive oxygen species (ROS) production. Our data showed that treatment with a molecular chaperone prevented SR Ca^{2+} handling defects and loss of myogenic tone and substantially attenuated spontaneous ICHs. These data provide evidence that impaired secretion of mutant collagen IV contributes to SMC Ca^{2+} signaling defects and cSVD pathology of *Col4a1*$^{+/G1344D}$ mice. The age dependency of the disease process may reflect the normal functional decline in SR protein homeostasis [61] that is exacerbated by mutant collagen in the SR. A systematic review of patients with *COL4A1* mutations revealed that the first presentation of the disease had a mean onset age of 36 years old [9]. This would suggest humans between 20-30 years old are able to compensate similarly to 3-month-old mice, but the ability to regulate misfolded proteins declines with age leading to increased SR stress.

We conclude that age-dependent disruption of Ca^{2+} signaling in SMCs due to impaired secretion of mutant collagen and diminished SR Ca^{2+} store load contributes to cSVD pathology in *Col4a1*$^{+/G1344D}$ mice. Future investigations into links between SMC SR stress and Ca^{2+} handling defects in other genetic and sporadic forms of cSVD may provide insight into novel pathogenic mechanisms.

Materials and Methods

Chemical and reagents:

Chemicals and other reagents were obtained from Sigma-Aldrich, Inc. (St. Louis, MO, USA) unless otherwise specified.

Animals:

Young adult (~3M) and middle-aged (~12M) male and female littermate *Col4a1*$^{+/+}$ and *Col4a1*$^{+/G1344D}$ mice were used in this study. The *Col4a1*^{G1344D} mutation was backcrossed to C57BL/6J mice for over 20 generations [62]. Animals were maintained in individually ventilated cages (≤5 mice/cage) with ad libitum access to food and water in a room with controlled 12-hour light and dark cycles. All animal care procedures and experimental protocols involving animals complied with the National Institutes of Health (NIH) *Guide for the Care and Use of Laboratory Animals* and were approved by the Institutional Animal Care and Use Committees at the University of Nevada, Reno, and University of California, San Francisco.

4PBA treatment:

Mice were provided with 4-phenylbutyrate (4PBA; 50 mM; Scandinavian Formulas Inc., Sellersville, PA, USA) from birth in drinking water that was refreshed weekly as described previously [26].

Histological analysis:

Isoflurane anesthetized mice were transcardially perfused with ice-cold phosphate-buffered saline (PBS) followed by ice cold 4% paraformaldehyde (Fisher, Waltham, MA, USA) in PBS. Brains were postfixed with 4% paraformaldehyde for 24 hours at 4°C, cryoprotected in 30% sucrose in PBS, and embedded in optimal cutting temperature compound (Fisher). Coronal cryosections (35 μm) regularly spaced (500 μm) along the rostrocaudal axis were stained with a Prussian blue and nuclear fast red stain kit (Abcam, Cambridge, UK) following the manufacturer's protocol. Images were acquired with a BZ-X700 microscope using BZ-X Viewer 1.3.0.5 software and stitched with BZ-X Analyzer 1.3.0.3 software (Keyence, Osaka, Japan). The percentage of brain area with Prussian blue staining for each section was calculated with ImageJ software (v2.3.0/1.53f; NIH, Bethesda, MD, USA). Hemorrhage severity was expressed as the percentage of hemosiderin surface area on ~21 sections for each brain (%) = [area of Prussian blue staining/total area of brain slices)] × 100.

In vivo magnetic resonance imaging:

In vivo magnetic resonance (MR) imaging was conducted on a 14.1 Tesla vertical MR system (Agilent Technologies, Palo-Alto, CA) equipped with 100 G/cm gradients and a single tuned millipede ^{1}H proton coil ($\varnothing_I$ = 40 mm). Before imaging, mice were anesthetized using isoflurane (1-1.5% in O_2), positioned in a dedicated cradle maintaining constant anesthesia, and placed in the MR bore; respiration and temperature were continuously monitored during all acquisitions to ensure animal well-being and data reproducibility. Susceptibility weighted imaging (SWI) was performed to acquire high-resolution images of the mouse brain using the following parameters: gradient-echo scheme, field of view (FOV) = 20x 20 mm^2, matrix = 256 x 256, 16 slices, 0.4 mm slice thickness, 0.1 mm interslice gap, number of averages = 16, echo time (TE)/repetition time (TR) = 4.60/140ms, flip angle = 10 degrees. T2-weighted (T2W) images were also acquired in a fast-spin-echo scheme to evaluate anatomical brain structures, using the same

FOV geometry as SWI and the following parameters: number of averages = 8, TE/TR = 21.38/2500ms, flip angle = 90 degrees. The fast-spin-echo based T2W imaging is less sensitive to distortion artifacts caused by B_0 inhomogeneity than SWI and is thus used for the atlas-based brain structure registration as described below.

Using in-house software, hypointense lesions corresponding to ICHs were quantified based on manual segmentation of the SWI images. To investigate the number and distribution of hypointense SWI lesions across the brain, an open-source atlas-based imaging data analysis pipeline (AIDAmri) [63] was customized to register T2W brain images to the Allen Brain Reference Atlas [64]. Based on the registration result, the normalized lesion volumes for each brain region were summed up across all animals and an intra-group region-wise volumetric analysis was performed.

Isolation of cerebral arteries and SMCs:

Mice were euthanized by decapitation under isoflurane anesthesia. Cerebral arteries were isolated from the brain in Ca^{2+}-free Mg^{2+} physiological saline solution (Mg^{2+}-PSS) consisting of 140 mM NaCl, 5 mM KCl, 2 mM $MgCl_2$, 10 mM HEPES, and 10 mM glucose (pH 7.4, adjusted with NaOH), with 0.5% bovine serum albumin (BSA). Native SMCs for patch-clamp experiments were obtained by initially digesting isolated arteries in 1 mg/mL papain (Worthington Biochemical Corporation, Lakewood, NJ, USA), 1 mg/mL dithiothreitol (DTT), and 10 mg/mL BSA in Ca^{2+}-free PSS at 37°C for 12 minutes, then incubating with 1 mg/mL type II collagenase (Worthington Biochemical Corporation) for 14 minutes. A single-cell suspension was prepared by washing digested arteries three times with Mg^{2+}-PSS and triturating with a fire-polished glass pipette. Cells used for this study were freshly dissociated on the day of experimentation.

Pressure myography:

The current best practice guidelines for pressure myography experiments were followed [32]. Arteries were mounted between two glass cannulas (outer diameter, 40–50 μm) in a pressure myograph chamber (Living Systems Instrumentation, St Albans City, VT, USA) and secured by a nylon thread. Intraluminal pressure was controlled with a servo-controlled peristaltic pump (Living Systems Instrumentation), and preparations were visualized with an inverted microscope (Accu-Scope Inc., Commack, NY, USA) coupled to a USB camera (The Imaging Source LLC, Charlotte, NC, USA). Changes in luminal diameter were assessed using IonWizard software (version 7.2.7.138; IonOptix LLC, Westwood, MA, USA). Arteries were bathed in warmed (37°C), oxygenated (21% O_2, 6% CO_2, 73% N_2) PSS (119 mM NaCl, 4.7 mM KCl, 21 mM $NaHCO_3$, 1.17 mM $MgSO_4$, 1.8 mM $CaCl_2$, 1.18 mM KH_2PO_4, 5 mM glucose, 0.03 mM EDTA) at an intraluminal pressure of 5 mmHg. Following equilibration for 15 min, intraluminal pressure was increased to 110 mmHg, and vessels were stretched to their approximate in vivo length, after which pressure was reduced back to 5 mmHg for an additional 15 min. Vessel viability was assessed for each preparation by evaluating vasoconstriction in response to high extracellular [K^+] PSS, made isotonic by adjusting [NaCl] (60 mM KCl, 63.7 mM NaCl). Arteries that showed less than 10% constriction in response to elevated [K^+] were excluded from further investigation.

Myogenic tone was assessed by raising the intraluminal pressure stepwise from 5 mmHg to 120 mmHg in 20 mmHg increments (5 to 20 mmHg for the first step). The active diameter was obtained by allowing vessels to equilibrate for at least 5 minutes at each pressure or until a steady-state diameter was reached. Following completion of the pressure-response study, intraluminal pressure was lowered to 5 mmHg, and arteries were superfused with Ca^{2+}-free PSS supplemented with EGTA (2 mM) and the voltage-dependent Ca^{2+} channel blocker diltiazem (10 μM) to inhibit SMC contraction, after which passive diameter was obtained by repeating the stepwise increase in intraluminal pressure. Myogenic tone at each pressure step was calculated as myogenic tone (%) = [1 – (active lumen diameter/passive lumen diameter)] × 100.

Membrane potential:

To measure SMC membrane potential, cerebral arteries were isolated, cannulated, and viability confirmed as described above. SMC membrane potential was recorded from intact pressurized arteries at intraluminal pressures of 20 mmHg and 80 mmHg. SMCs were impaled through the adventitia with glass intracellular microelectrodes (100-200 MΩ) backfilled with 3M KCl. Membrane potential was recorded using an Electro 705 amplifier (World Precision Instruments, Sarasota, FL, USA). Analog output from the amplifier was recorded using Ionwizard software (version 7.5.1.162; IonOptix). Criteria for acceptance of membrane potential recordings were (i) an abrupt negative deflection of potential as the microelectrode was advanced into a cell, (ii) stable membrane potential for at least 30 seconds, and (iii) an abrupt change in the potential to ~0 mV after the electrode was retracted from the cell.

Electrophysiological recordings:

Enzymatically isolated native SMCs were transferred to a recording chamber (Warner Instruments, Holliston, MA, USA) and allowed to adhere to glass coverslips for 20 minutes at room temperature. Recording electrodes (3–5 MΩ) were pulled on a model P-87 micropipette puller (Sutter Instruments, Novato, CA, USA) and polished with a MF-830 MicroForge (Narishige Scientific Instruments Laboratories, Long Island, NY, USA). Currents were recorded at room temperature using an Axopatch 200B amplifier (Molecular Devices, Sunnyvale, CA, USA) equipped with an Axon CV 203BU headstage and Digidata 1440A digitizer (Molecular Devices) for all patch-clamp electrophysiology experiments. Clampex and Clampfit (version 10.2; Molecular Devices) were used for data acquisition and analysis.

The bathing solution composition for perforated-patch recordings of Kv currents, STOCs, and TICCs was 134 mM NaCl, 6 mM KCl, 1 mM $MgCl_2$, 2 mM $CaCl_2$, 10 mM HEPES, and 10 mM glucose (pH 7.4, adjusted with NaOH). The patch pipette solution contained 110 mM K-aspartate, 1 mM $MgCl_2$, 30 mM KCl, 10 mM NaCl, 10 mM HEPES, and 5 μM EGTA (pH 7.2, adjusted with KOH). Amphotericin B (200 μM) was included in the pipette solution to enable electrical access. Whole-cell K^+ currents were recorded using a step protocol (−60 to +60 mV in 10 mV, 250 ms steps) from a holding potential of −80 mV. The BK channel blocker paxilline (1 μM) was included in the bath solution when Kv currents were recorded. Whole-cell K^+ currents were recorded in the absence and presence

of K_V channel blocker 4-aminopyridine (5 mM), and the Kv component was determined by subtraction. Summary current-voltage (I-V) plots were generated using values obtained from the last 50 ms of each step. STOCs were recorded from SMCs voltage-clamped over a range of membrane potentials (−60 to 0 mV; 10 mV steps). TICCs were recorded from SMCs voltage-clamped at −70 mV; membrane stretch was delivered by applying negative pressure through the recording electrode using a pressure clamp system (HSPC-1; ALA Scientific Instruments Inc., Farmingdale, NY, USA). TICC activity was calculated as the sum of the open channel probability (NP_o) of multiple open states of 1.75 pA [65].

Whole-cell BK currents were recorded in the same bath solution Kv currents, STOCs, and TICCs, but the patch pipette solution contained 140 mM KCl, 1.9 mM $MgCl_2$, 0.075 mM $CaCl_2$, 10 mM HEPES, 2 mM Na_2ATP, and 0.1 mM EGTA (pH 7.2, adjusted with KOH). Whole-cell K^+ currents were recorded using a step protocol (−100 to +100 mV in 20 mV, 500 ms steps) from a holding potential of −80 mV. Whole-cell K^+ currents were recorded in the absence and presence of the BK channel blocker paxilline (1 μM) and the BK component was determined by subtraction. Summary current-voltage (I-V) plots were generated using values obtained from the last 50 ms of each step.

Whole-cell TRPM4 currents were recorded in a bath solution consisting of 156 mM NaCl, 1.5 mM $CaCl_2$, 10 mM glucose, 10 mM HEPES, and 10 mM TEACl (pH 7.4, adjusted with NaOH). The patch pipette solution contained 156 mM CsCl, 8 mM NaCl, 1 mM $MgCl_2$, 10 mM HEPES (pH 7.4, adjusted with NaOH), and a free Ca^{2+} concentration of 200 μM, adjusted using the appropriate amounts of $CaCl_2$ and EGTA, as determined with Max-Chelator software (WEBMAXC standard). Whole-cell cation currents were evoked by applying 400 ms voltage ramps from −100 to +100 mV from a holding potential of −60 mV. Voltage ramps were repeated every 2 s for 300 s. The selective TRPM4 inhibitor 9-phenanthrol (30 μM) was applied after peak TRPM4 current was recorded (~100 s). Whole-cell TRPM4 current amplitude was expressed as the 9-phenanthrol-sensitive current at +100 mV.

Quantitative droplet digital PCR:

Total RNA was extracted from isolated cerebral arteries by homogenization in TRIzol reagent (Invitrogen, Waltham, MA, USA), followed by purification using a Direct-zol RNA microprep kit (Zymo Research, Irvine, CA, USA) with on-column DNAse treatment. RNA concentration was determined using an RNA 6000 Pico Kit run on a Bioanalyzer 2100 running Agilent 2100 Expert Software (B.02.11; Agilent Technologies, Santa Clara, CA, USA). RNA was converted to cDNA with iScript cDNA Supermix (Bio-Rad, Hercules, CA, USA). Quantitative droplet digital PCR (ddPCR) was performed using QX200 ddPCR EvaGreen Supermix (Bio-Rad), custom-designed primers (Supplementary Table 1), and cDNA templates. Generated droplet emulsions were amplified using a C100 Touch Thermal Cycler (Bio-Rad), and the fluorescence intensities of individual droplets were measured with a QX200 Droplet Reader (Bio-Rad) running QuantaSoft (version 1.7.4; Bio-Rad). Analysis was performed with QuantaSoft Analysis Pro (version 1.0596; Bio-Rad).

Ca^{2+} imaging:

Images were acquired using an iXon 897 EMCCD camera (Andor; 16 × 16 μm pixel size) coupled to a spinning-disk confocal head (CSU-X1; Yokogawa) with a 100× oil-immersion objective (Olympus; NA 1.45) at an acquisition rate of 33 frames per second (fps). Custom software (SparkAn) provided by Dr. Adrian D. Bonev (University of Vermont) was used to analyze the properties of Ca^{2+} sparks and whole-cell RyR and IP_3R Ca^{2+} signals.

To image Ca^{2+} sparks, a suspension of freshly isolated SMCs was placed in a glass-bottom 35 mm dish, and cells were allowed to adhere to the glass coverslip for 20 min at room temperature. SMCs were loaded with the Ca^{2+}-sensitive fluorophore Fluo-4-AM (1 μM; Invitrogen) in the dark for 20 minutes at room temperature in Mg^{2+}-PSS, washed three times with Ca^{2+}-containing PSS, and incubated at room temperature for 20 min in the dark to allow sufficient time for Fluo-4 de-esterification. The threshold for Ca^{2+} spark detection was defined as local increases in fluorescence ≥0.2 $\Delta F/F_0$.

To image RyR and IP_3R Ca^{2+} signals, SMCs were plated and loaded with Fluo-4-AM as stated above, but immediately before imaging, cells were washed three times and imaged in Mg^{2+}-PSS to eliminate signals resulting from Ca^{2+} influx. Caffeine (10 mM) or U46619 (100 nM; Enzo Biochem, Farmingdale, NY) was applied to the bath.

Statistical analysis:

Summary data are presented as means ± SEM. Statistical analyses were performed, and graphs were constructed using Prism version 9.3.1 (GraphPad Software, San Diego, CA, USA). The value of n refers to the number of cells for patch-clamp electrophysiology and Ca^{2+} imaging experiments, the number of arteries for pressure myography and membrane potential experiments, and the number of animals for histological analyses, magnetic resonance imaging, and ddPCR experiments. Statistical analyses were performed using unpaired Student's t-tests and one-way and two-way analysis of variance (ANOVA). A P value < 0.05 was considered statistically significant for all analyses.

Supplementary Material

Refer to Web version on PubMed Central for supplementary material.

Funding:

This study was supported by grants from the National Institutes of Health (NHLBI R35HL155008, R01HL091905, R01HL137852, R01HL139585, R01146054, and R01HL122770, NIGMS P20GM130459 to S.E., and NINDS RF1NS110044 and R33NS115132 to M.M.C, D.B.G, and S.E.; The Transgenic Genotyping and Phenotyping Core at the COBRE Center for Molecular and Cellular Signaling in the Cardiovascular System, University of Nevada, Reno, is maintained by a grant from NIH/NIGMS (P20GM130459 Sub#5451), as is the High Spatial and Temporal Resolution Imaging Core at the COBRE Center for Molecular and Cellular Signaling in the Cardiovascular System, University of Nevada, Reno (P20GM130459 Sub#5452). The UCSF Department of Ophthalmology is supported by P30EY002162 and an unrestricted grant from Research to Prevent Blindness.

Data and materials availability:

All data needed to evaluate the conclusions in the paper are present in the paper or the Supplementary Materials. Processed data are available on DRYAD (https://datadryad.org/

stash/dataset/doi:10.5061/dryad.k3j9kd5dz). *Col4a1* mutant mice are available from D.B.G. under a material transfer agreement with UCSF.

References and Notes

1. Markus HS. Genes, endothelial function and cerebral small vessel disease in man. Exp Physiol. 2008;93:121–127. doi: 10.1113/expphysiol.2007.038752 [PubMed: 17933861]
2. Pantoni L. Cerebral small vessel disease: from pathogenesis and clinical characteristics to therapeutic challenges. Lancet Neurol. 2010;9:689–701. doi: 10.1016/S1474-4422(10)70104-6 [PubMed: 20610345]
3. Choi JC. Genetics of cerebral small vessel disease. J Stroke. 2015;17:7–16. doi: 10.5853/jos.2015.17.1.7 [PubMed: 25692103]
4. Joutel A, Faraci FM. Cerebral small vessel disease: insights and opportunities from mouse models of collagen IV-related small vessel disease and cerebral autosomal dominant arteriopathy with subcortical infarcts and leukoencephalopathy. Stroke. 2014;45:1215–1221. doi: 10.1161/STROKEAHA.113.002878 [PubMed: 24503668]
5. Joutel A, Haddad I, Ratelade J, Nelson MT. Perturbations of the cerebrovascular matrisome: A convergent mechanism in small vessel disease of the brain? J Cereb Blood Flow Metab. 2016;36:143–157. doi: 10.1038/jcbfm.2015.62 [PubMed: 25853907]
6. Rutten-Jacobs LC, Traylor M, Adib-Samii P, Thijs V, Sudlow C, Rothwell PM, Boncoraglio G, Dichgans M, Bevan S, Meschia J, et al. Common NOTCH3 Variants and Cerebral Small-Vessel Disease. Stroke. 2015;46:1482–1487. doi: 10.1161/STROKEAHA.114.008540 [PubMed: 25953367]
7. Gould DB, Phalan FC, Breedveld GJ, van Mil SE, Smith RS, Schimenti JC, Aguglia U, van der Knaap MS, Heutink P, John SW. Mutations in Col4a1 cause perinatal cerebral hemorrhage and porencephaly. Science. 2005;308:1167–1171. doi: 10.1126/science.1109418 [PubMed: 15905400]
8. Gould DB, Phalan FC, van Mil SE, Sundberg JP, Vahedi K, Massin P, Bousser MG, Heutink P, Miner JH, Tournier-Lasserve E, et al. Role of COL4A1 in small-vessel disease and hemorrhagic stroke. N Engl J Med. 2006;354:1489–1496. doi: 10.1056/NEJMoa053727 [PubMed: 16598045]
9. Lanfranconi S, Markus HS. COL4A1 mutations as a monogenic cause of cerebral small vessel disease: a systematic review. Stroke. 2010;41:e513–518. doi: 10.1161/STROKEAHA.110.581918 [PubMed: 20558831]
10. Jeanne M, Jorgensen J, Gould DB. Molecular and Genetic Analyses of Collagen Type IV Mutant Mouse Models of Spontaneous Intracerebral Hemorrhage Identify Mechanisms for Stroke Prevention. Circulation. 2015;131:1555–1565. doi: 10.1161/CIRCULATIONAHA.114.013395 [PubMed: 25753534]
11. Jeanne M, Labelle-Dumais C, Jorgensen J, Kauffman WB, Mancini GM, Favor J, Valant V, Greenberg SM, Rosand J, Gould DB. COL4A2 mutations impair COL4A1 and COL4A2 secretion and cause hemorrhagic stroke. Am J Hum Genet. 2012;90:91–101. doi: 10.1016/j.ajhg.2011.11.022 [PubMed: 22209247]
12. Gould DB, Marchant JK, Savinova OV, Smith RS, John SW. Col4a1 mutation causes endoplasmic reticulum stress and genetically modifiable ocular dysgenesis. Hum Mol Genet. 2007;16:798–807. doi: 10.1093/hmg/ddm024 [PubMed: 17317786]
13. Kuo DS, Labelle-Dumais C, Mao M, Jeanne M, Kauffman WB, Allen J, Favor J, Gould DB. Allelic heterogeneity contributes to variability in ocular dysgenesis, myopathy and brain malformations caused by Col4a1 and Col4a2 mutations. Hum Mol Genet. 2014;23:1709–1722. doi: 10.1093/hmg/ddt560 [PubMed: 24203695]
14. Davis MJ, Hill MA. Signaling mechanisms underlying the vascular myogenic response. Physiol Rev. 1999;79:387–423. doi: 10.1152/physrev.1999.79.2.387 [PubMed: 10221985]
15. Gonzales AL, Garcia ZI, Amberg GC, Earley S. Pharmacological inhibition of TRPM4 hyperpolarizes vascular smooth muscle. Am J Physiol Cell Physiol. 2010;299:C1195–1202. doi: 10.1152/ajpcell.00269.2010 [PubMed: 20826763]

16. Earley S, Waldron BJ, Brayden JE. Critical role for transient receptor potential channel TRPM4 in myogenic constriction of cerebral arteries. Circ Res. 2004;95:922–929. doi: 10.1161/01.RES.0000147311.54833.03 [PubMed: 15472118]

17. Reading SA, Brayden JE. Central role of TRPM4 channels in cerebral blood flow regulation. Stroke. 2007;38:2322–2328. doi: 10.1161/STROKEAHA.107.483404 [PubMed: 17585083]

18. Nelson MT, Cheng H, Rubart M, Santana LF, Bonev AD, Knot HJ, Lederer WJ. Relaxation of arterial smooth muscle by calcium sparks. Science. 1995;270:633–637. doi: 10.1126/science.270.5236.633 [PubMed: 7570021]

19. Knot HJ, Standen NB, Nelson MT. Ryanodine receptors regulate arterial diameter and wall [Ca2+] in cerebral arteries of rat via Ca2+-dependent K+ channels. J Physiol. 1998;508 (Pt 1):211–221. doi: 10.1111/j.1469-7793.1998.211br.x [PubMed: 9490841]

20. Jackson WF. Potassium Channels in Regulation of Vascular Smooth Muscle Contraction and Growth. Adv Pharmacol. 2017;78:89–144. doi: 10.1016/bs.apha.2016.07.001 [PubMed: 28212804]

21. Gonzales AL, Amberg GC, Earley S. Ca2+ release from the sarcoplasmic reticulum is required for sustained TRPM4 activity in cerebral artery smooth muscle cells. Am J Physiol Cell Physiol. 2010;299:C279–288. doi: 10.1152/ajpcell.00550.2009 [PubMed: 20427713]

22. Dabertrand F, Kroigaard C, Bonev AD, Cognat E, Dalsgaard T, Domenga-Denier V, Hill-Eubanks DC, Brayden JE, Joutel A, Nelson MT. Potassium channelopathy-like defect underlies early-stage cerebrovascular dysfunction in a genetic model of small vessel disease. Proc Natl Acad Sci U S A. 2015;112:E796–805. doi: 10.1073/pnas.1420765112 [PubMed: 25646445]

23. Murray LS, Lu Y, Taggart A, Van Regemorter N, Vilain C, Abramowicz M, Kadler KE, Van Agtmael T. Chemical chaperone treatment reduces intracellular accumulation of mutant collagen IV and ameliorates the cellular phenotype of a COL4A2 mutation that causes haemorrhagic stroke. Hum Mol Genet. 2014;23:283–292. doi: 10.1093/hmg/ddt418 [PubMed: 24001601]

24. Malo A, Kruger B, Goke B, Kubisch CH. 4-Phenylbutyric acid reduces endoplasmic reticulum stress, trypsin activation, and acinar cell apoptosis while increasing secretion in rat pancreatic acini. Pancreas. 2013;42:92–101. doi: 10.1097/MPA.0b013e318259f6ca [PubMed: 22889983]

25. Perlmutter DH. Chemical chaperones: a pharmacological strategy for disorders of protein folding and trafficking. Pediatr Res. 2002;52:832–836. doi: 10.1203/00006450-200212000-00004 [PubMed: 12438657]

26. Hayashi G, Labelle-Dumais C, Gould DB. Use of sodium 4-phenylbutyrate to define therapeutic parameters for reducing intracerebral hemorrhage and myopathy in Col4a1 mutant mice. Dis Model Mech. 2018;11. doi: 10.1242/dmm.034157

27. Cannistraro RJ, Badi M, Eidelman BH, Dickson DW, Middlebrooks EH, Meschia JF. CNS small vessel disease: A clinical review. Neurology. 2019;92:1146–1156. doi: 10.1212/WNL.0000000000007654 [PubMed: 31142635]

28. Hilal S, Mok V, Youn YC, Wong A, Ikram MK, Chen CL. Prevalence, risk factors and consequences of cerebral small vessel diseases: data from three Asian countries. J Neurol Neurosurg Psychiatry. 2017;88:669–674. doi: 10.1136/jnnp-2016-315324 [PubMed: 28600443]

29. Meuwissen ME, Halley DJ, Smit LS, Lequin MH, Cobben JM, de Coo R, van Harssel J, Sallevelt S, Woldringh G, van der Knaap MS, et al. The expanding phenotype of COL4A1 and COL4A2 mutations: clinical data on 13 newly identified families and a review of the literature. Genet Med. 2015;17:843–853. doi: 10.1038/gim.2014.210 [PubMed: 25719457]

30. Yamasaki E, Ali S, Sanchez Solano A, Thakore P, Smith M, Wang X, Labelle-Dumais C, Gould DB, Earley S. Faulty TRPM4 channels underlie age-dependent cerebral vascular dysfunction in Gould syndrome. Proc Natl Acad Sci U S A. 2023;120:e2217327120. doi: 10.1073/pnas.2217327120 [PubMed: 36693102]

31. Shi Y, Wardlaw JM. Update on cerebral small vessel disease: a dynamic whole-brain disease. Stroke Vasc Neurol. 2016;1:83–92. doi: 10.1136/svn-2016-000035 [PubMed: 28959468]

32. Wenceslau CF, McCarthy CG, Earley S, England SK, Filosa JA, Goulopoulou S, Gutterman DD, Isakson BE, Kanagy NL, Martinez-Lemus LA, et al. Guidelines for the measurement of vascular function and structure in isolated arteries and veins. Am J Physiol Heart Circ Physiol. 2021;321:H77–H111. doi: 10.1152/ajpheart.01021.2020 [PubMed: 33989082]

33. Harder DR. Pressure-dependent membrane depolarization in cat middle cerebral artery. Circ Res. 1984;55:197–202. doi: 10.1161/01.res.55.2.197 [PubMed: 6744529]
34. Knot HJ, Nelson MT. Regulation of arterial diameter and wall [Ca2+] in cerebral arteries of rat by membrane potential and intravascular pressure. J Physiol. 1998;508 (Pt 1):199–209. doi: 10.1111/j.1469-7793.1998.199br.x [PubMed: 9490839]
35. Pritchard HAT, Gonzales AL, Pires PW, Drumm BT, Ko EA, Sanders KM, Hennig GW, Earley S. Microtubule structures underlying the sarcoplasmic reticulum support peripheral coupling sites to regulate smooth muscle contractility. Sci Signal. 2017;10. doi: 10.1126/scisignal.aan2694
36. Brayden JE, Nelson MT. Regulation of arterial tone by activation of calcium-dependent potassium channels. Science. 1992;256:532–535. doi: 10.1126/science.1373909 [PubMed: 1373909]
37. Launay P, Fleig A, Perraud AL, Scharenberg AM, Penner R, Kinet JP. TRPM4 is a Ca2+-activated nonselective cation channel mediating cell membrane depolarization. Cell. 2002;109:397–407. doi: 10.1016/s0092-8674(02)00719-5 [PubMed: 12015988]
38. Gonzales AL, Yang Y, Sullivan MN, Sanders L, Dabertrand F, Hill-Eubanks DC, Nelson MT, Earley S. A PLCgamma1-dependent, force-sensitive signaling network in the myogenic constriction of cerebral arteries. Sci Signal. 2014;7:ra49. doi: 10.1126/scisignal.2004732 [PubMed: 24866019]
39. Earley S, Straub SV, Brayden JE. Protein kinase C regulates vascular myogenic tone through activation of TRPM4. Am J Physiol Heart Circ Physiol. 2007;292:H2613–2622. doi: 10.1152/ajpheart.01286.2006 [PubMed: 17293488]
40. Nilius B, Prenen J, Droogmans G, Voets T, Vennekens R, Freichel M, Wissenbach U, Flockerzi V. Voltage dependence of the Ca2+-activated cation channel TRPM4. J Biol Chem. 2003;278:30813–30820. doi: 10.1074/jbc.M305127200 [PubMed: 12799367]
41. Pires PW, Ko EA, Pritchard HAT, Rudokas M, Yamasaki E, Earley S. The angiotensin II receptor type 1b is the primary sensor of intraluminal pressure in cerebral artery smooth muscle cells. J Physiol. 2017;595:4735–4753. doi: 10.1113/JP274310 [PubMed: 28475214]
42. Yamasaki E, Thakore P, Krishnan V, Earley S. Differential expression of angiotensin II type 1 receptor subtypes within the cerebral microvasculature. Am J Physiol Heart Circ Physiol. 2020;318:H461–H469. doi: 10.1152/ajpheart.00582.2019 [PubMed: 31886721]
43. Schleifenbaum J, Kassmann M, Szijarto IA, Hercule HC, Tano JY, Weinert S, Heidenreich M, Pathan AR, Anistan YM, Alenina N, et al. Stretch-activation of angiotensin II type 1a receptors contributes to the myogenic response of mouse mesenteric and renal arteries. Circ Res. 2014;115:263–272. doi: 10.1161/CIRCRESAHA.115.302882 [PubMed: 24838176]
44. Yasuda N, Miura S, Akazawa H, Tanaka T, Qin Y, Kiya Y, Imaizumi S, Fujino M, Ito K, Zou Y, et al. Conformational switch of angiotensin II type 1 receptor underlying mechanical stress-induced activation. EMBO Rep. 2008;9:179–186. doi: 10.1038/sj.embor.7401157 [PubMed: 18202720]
45. McPherson PS, Kim YK, Valdivia H, Knudson CM, Takekura H, Franzini-Armstrong C, Coronado R, Campbell KP. The brain ryanodine receptor: a caffeine-sensitive calcium release channel. Neuron. 1991;7:17–25. doi: 10.1016/0896-6273(91)90070-g [PubMed: 1648939]
46. Wray S, Burdyga T. Sarcoplasmic reticulum function in smooth muscle. Physiol Rev. 2010;90:113–178. doi: 10.1152/physrev.00018.2008 [PubMed: 20086075]
47. Branyan K, Labelle-Dumais C, Wang X, Hayashi G, Lee B, Peltz Z, Gorman S, Li BQ, Mao M, Gould DB. Elevated TGFbeta signaling contributes to cerebral small vessel disease in mouse models of Gould syndrome. Matrix Biol. 2023;115:48–70. doi: 10.1016/j.matbio.2022.11.007 [PubMed: 36435425]
48. Iannitti T, Palmieri B. Clinical and experimental applications of sodium phenylbutyrate. Drugs R D. 2011;11:227–249. doi: 10.2165/11591280-000000000-00000 [PubMed: 21902286]
49. Bordes S, Werner C, Mathkour M, McCormack E, Iwanaga J, Loukas M, Lammle M, Dumont AS, Tubbs RS. Arterial Supply of the Thalamus: A Comprehensive Review. World Neurosurg. 2020;137:310–318. doi: 10.1016/j.wneu.2020.01.237 [PubMed: 32036065]
50. Joutel A, Monet-Lepretre M, Gosele C, Baron-Menguy C, Hammes A, Schmidt S, Lemaire-Carrette B, Domenga V, Schedl A, Lacombe P, et al. Cerebrovascular dysfunction and microcirculation rarefaction precede white matter lesions in a mouse genetic model of cerebral

ischemic small vessel disease. J Clin Invest. 2010;120:433–445. doi: 10.1172/JCI39733 [PubMed: 20071773]

51. Nelson MT, Quayle JM. Physiological roles and properties of potassium channels in arterial smooth muscle. Am J Physiol. 1995;268:C799–822. doi: 10.1152/ajpcell.1995.268.4.C799 [PubMed: 7733230]
52. Krishnan V, Ali S, Gonzales AL, Thakore P, Griffin CS, Yamasaki E, Alvarado MG, Johnson MT, Trebak M, Earley S. STIM1-dependent peripheral coupling governs the contractility of vascular smooth muscle cells. Elife. 2022;11. doi: 10.7554/eLife.70278
53. McCarron JG, Craig JW, Bradley KN, Muir TC. Agonist-induced phasic and tonic responses in smooth muscle are mediated by InsP(3). J Cell Sci. 2002;115:2207–2218. doi: 10.1242/jcs.115.10.2207 [PubMed: 11973361]
54. Shmygol A, Wray S. Modulation of agonist-induced Ca2+ release by SR Ca2+ load: direct SR and cytosolic Ca2+ measurements in rat uterine myocytes. Cell Calcium. 2005;37:215–223. doi: 10.1016/j.ceca.2004.10.002 [PubMed: 15670868]
55. Parekh AB, Putney JW, Jr. Store-operated calcium channels. Physiol Rev. 2005;85:757–810. doi: 10.1152/physrev.00057.2003 [PubMed: 15788710]
56. Fernandez RA, Wan J, Song S, Smith KA, Gu Y, Tauseef M, Tang H, Makino A, Mehta D, Yuan JX. Upregulated expression of STIM2, TRPC6, and Orai2 contributes to the transition of pulmonary arterial smooth muscle cells from a contractile to proliferative phenotype. Am J Physiol Cell Physiol. 2015;308:C581–593. doi: 10.1152/ajpcell.00202.2014 [PubMed: 25673771]
57. Potier M, Gonzalez JC, Motiani RK, Abdullaev IF, Bisaillon JM, Singer HA, Trebak M. Evidence for STIM1- and Orai1-dependent store-operated calcium influx through ICRAC in vascular smooth muscle cells: role in proliferation and migration. FASEB J. 2009;23:2425–2437. doi: 10.1096/fj.09-131128 [PubMed: 19364762]
58. Schroder M, Kaufman RJ. The mammalian unfolded protein response. Annu Rev Biochem. 2005;74:739–789. doi: 10.1146/annurev.biochem.73.011303.074134 [PubMed: 15952902]
59. Lebeau PF, Platko K, Byun JH, Austin RC. Calcium as a reliable marker for the quantitative assessment of endoplasmic reticulum stress in live cells. J Biol Chem. 2021;296:100779. doi: 10.1016/j.jbc.2021.100779 [PubMed: 34000299]
60. Yamamoto WR, Bone RN, Sohn P, Syed F, Reissaus CA, Mosley AL, Wijeratne AB, True JD, Tong X, Kono T, et al. Endoplasmic reticulum stress alters ryanodine receptor function in the murine pancreatic beta cell. J Biol Chem. 2019;294:168–181. doi: 10.1074/jbc.RA118.005683 [PubMed: 30420428]
61. Chadwick SR, Lajoie P. Endoplasmic Reticulum Stress Coping Mechanisms and Lifespan Regulation in Health and Diseases. Front Cell Dev Biol. 2019;7:84. doi: 10.3389/fcell.2019.00084 [PubMed: 31231647]
62. Favor J, Gloeckner CJ, Janik D, Klempt M, Neuhauser-Klaus A, Pretsch W, Schmahl W, Quintanilla-Fend L. Type IV procollagen missense mutations associated with defects of the eye, vascular stability, the brain, kidney function and embryonic or postnatal viability in the mouse, Mus musculus: an extension of the Col4a1 allelic series and the identification of the first two Col4a2 mutant alleles. Genetics. 2007;175:725–736. doi: 10.1534/genetics.106.064733 [PubMed: 17179069]
63. Pallast N, Diedenhofen M, Blaschke S, Wieters F, Wiedermann D, Hoehn M, Fink GR, Aswendt M. Processing Pipeline for Atlas-Based Imaging Data Analysis of Structural and Functional Mouse Brain MRI (AIDAmri). Front Neuroinform. 2019;13:42. doi: 10.3389/fninf.2019.00042 [PubMed: 31231202]
64. Dong HW. Allen reference atlas : a digital color brain atlas of the C57Black/6J male mouse. Hoboken, N.J.: Wiley; 2008.
65. Gonzales AL, Amberg GC, Earley S. Ca2+ release from the sarcoplasmic reticulum is required for sustained TRPM4 activity in cerebral artery smooth muscle cells. American journal of physiology Cell physiology. 2010;299:C279–288. [PubMed: 20427713]

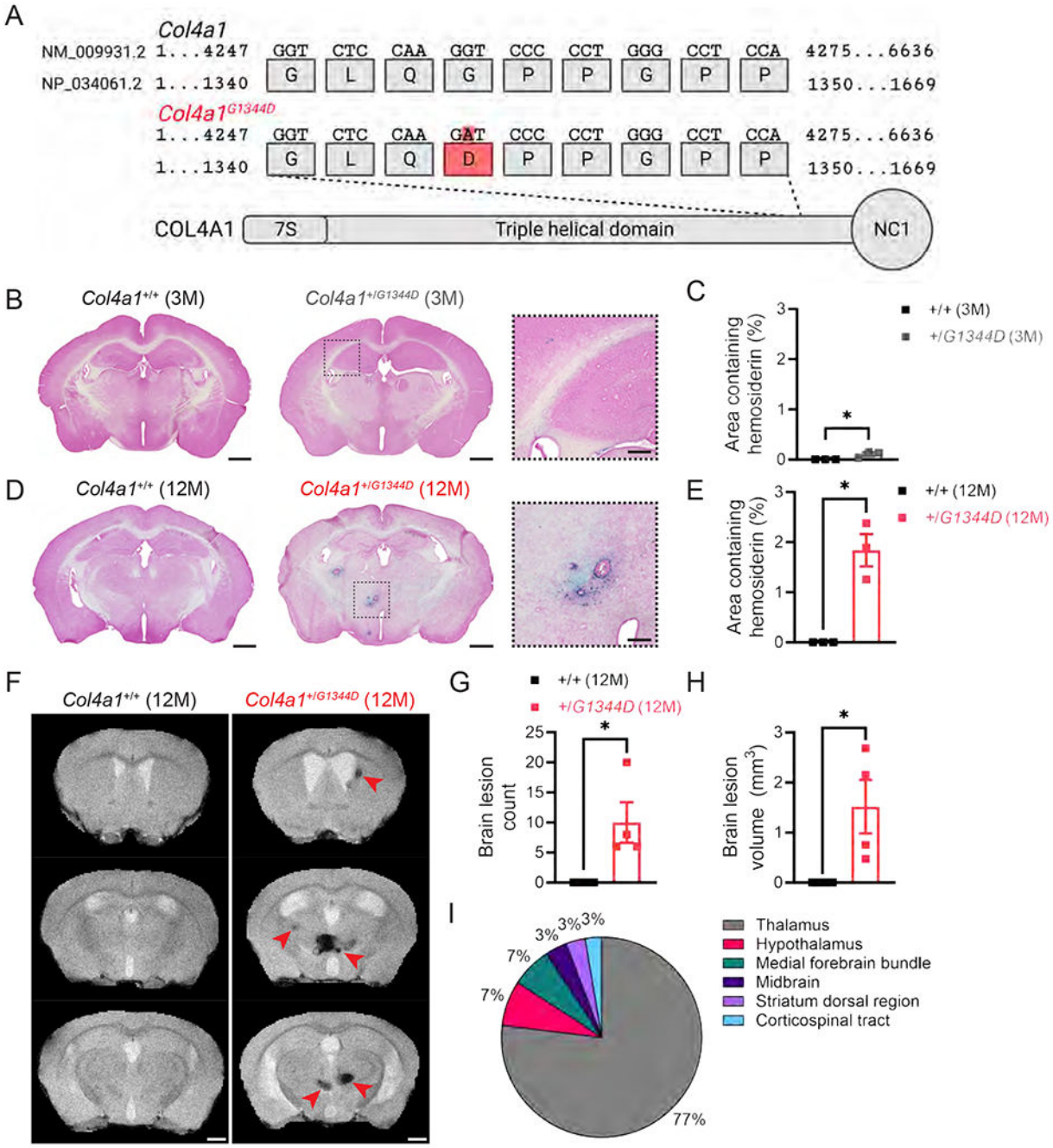

Figure 1. *Col4a1*$^{+/G1344D}$ mice exhibit age-dependent pathologies.

(A) Schematic representation of the *Col4a1* point mutation that leads to *Col4a1*^{G1344D}. **(B)** Intracerebral hemorrhages (ICHs) were assessed using Prussian blue staining. Representative images of brain sections from 3 M-old *Col4a1*$^{+/+}$ and *Col4a1*$^{+/G1344D}$ mice stained with Prussian blue. **(C)** Summary data presented as percentage of brain area with Prussian blue staining in brain sections (500 μm intervals). N = 3 animals per group. *P ≤ 0.05, unpaired t-test. **(D)** Representative images of brain sections from 12 M-old *Col4a1*$^{+/+}$ and *Col4a1*$^{+/G1344D}$ mice stained with Prussian blue. **(E)** Summary data presented

as percentage of brain area with Prussian blue staining in brain sections (500 μm intervals). N = 3 animals per group. *P ≤ 0.05, unpaired t-test. **(F)** Brain lesions were evaluated in vivo with high-field susceptibility-weighted magnetic resonance imaging (SWI). Representative SWI images from 12 M-old *Col4a1*$^{+/+}$ and *Col4a1*$^{+/G1344D}$ mice. Red arrowheads highlight hypointense pixels that indicate hemorrhagic lesions. **(G and H)** Quantification of the number of lesions (G) and the total volume of lesions detected by SWI (H). N = 4 animals per group. *P ≤ 0.05, unpaired t-test. **(I)** Region-wise volumetric distribution of lesions detected by SWI from 12 M-old *Col4a1*$^{+/G1344D}$ mice. Scale bars = 1 mm. Inset scale bars = 250 μm.

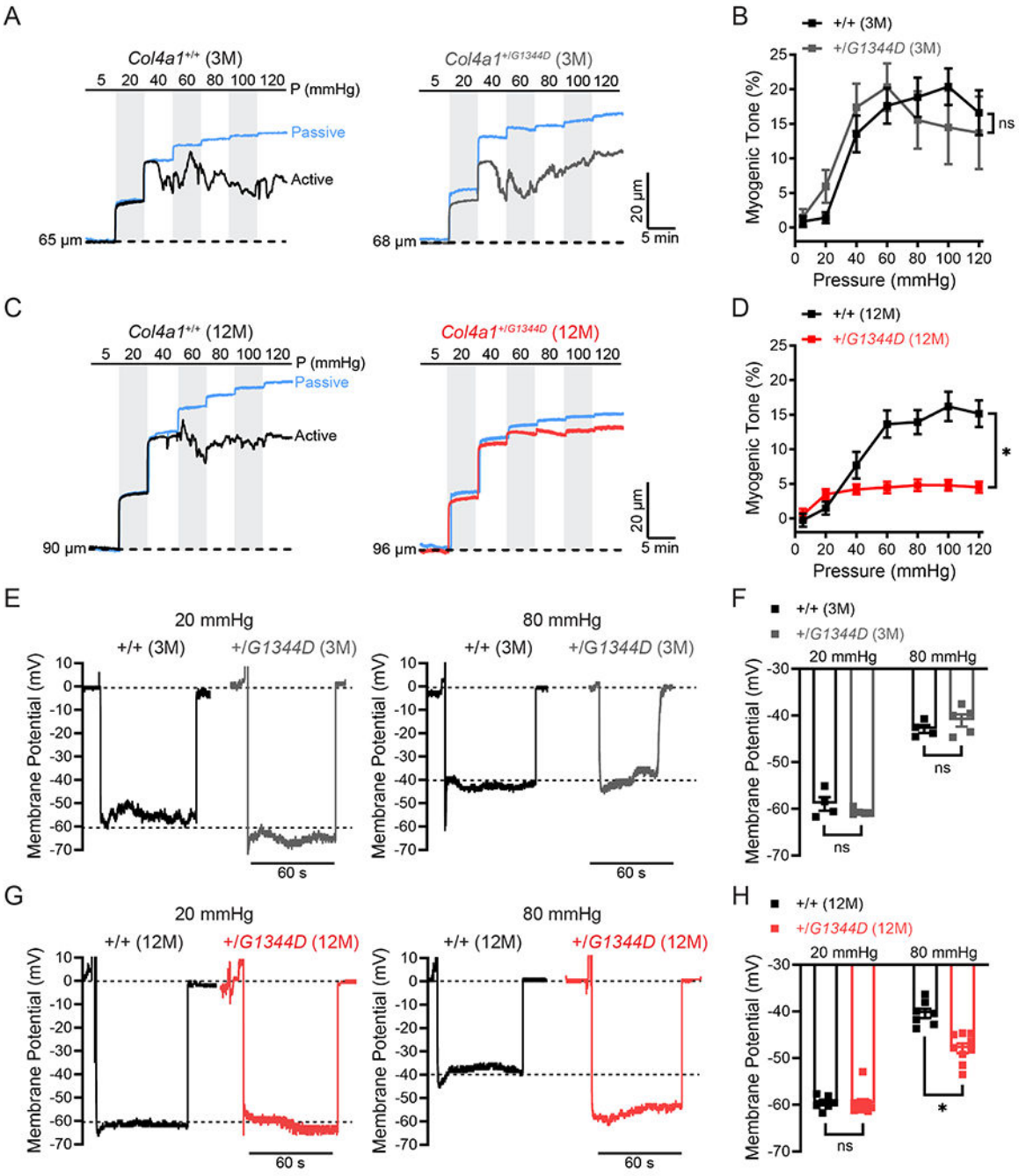

Figure 2. Diminished pressure-induced constriction of cerebral arteries from 12 M-old *Col4a1*$^{+/G1344D}$ mice is due to impaired SMC membrane depolarization.

(A) Representative recordings of the inner diameter of isolated cerebral arteries from 3 M-old *Col4a1*$^{+/+}$ and *Col4a1*$^{+/G1344D}$ mice show the myogenic response to increased pressure (active) and the dilation of the same arteries when extracellular Ca^{2+} has been removed (passive). **(B)** Summary data of myogenic tone as a function of intraluminal pressure. n = 5-10 vessels from 5 or 6 animals per group. ns = not significant, two-way ANOVA. **(C)** Representative recordings of the inner diameter of isolated cerebral arteries from 12

M-old *Col4a1*$^{+/+}$ and *Col4a1*$^{+/G1344D}$ mice. **(D)** Summary data of myogenic tone as a function of intraluminal pressure. n = 13 vessels from 6 or 9 animals per group. *P ≤ 0.05, two-way ANOVA. **(E)** Representative membrane potential (mV) recordings of smooth muscle cells (SMCs) in pressurized cerebral arteries isolated from 3 M-old *Col4a1*$^{+/+}$ and *Col4a1*$^{+/G1344D}$ mice at 20 mmHg and 80 mmHg intraluminal pressure. **(F)** Summary data showing membrane potential of SMCs in pressurized cerebral arteries at 20 mmHg and 80 mmHg intraluminal pressure. n = 4-5 vessels from 3 or 4 animals per group. ns = not significant, unpaired t-test. **(G)** Representative membrane potential recordings of SMCs in pressurized cerebral arteries isolated from 12 M-old *Col4a1*$^{+/+}$ and *Col4a1*$^{+/G1344D}$ mice at 20 mmHg and 80 mmHg intraluminal pressure. **(H)** Summary data showing membrane potential of SMCs in pressurized cerebral arteries at 20 mmHg and 80 mmHg intraluminal pressure. n = 7-9 vessels from 5 or 6 mice per group. *P ≤ 0.05, unpaired t-test.

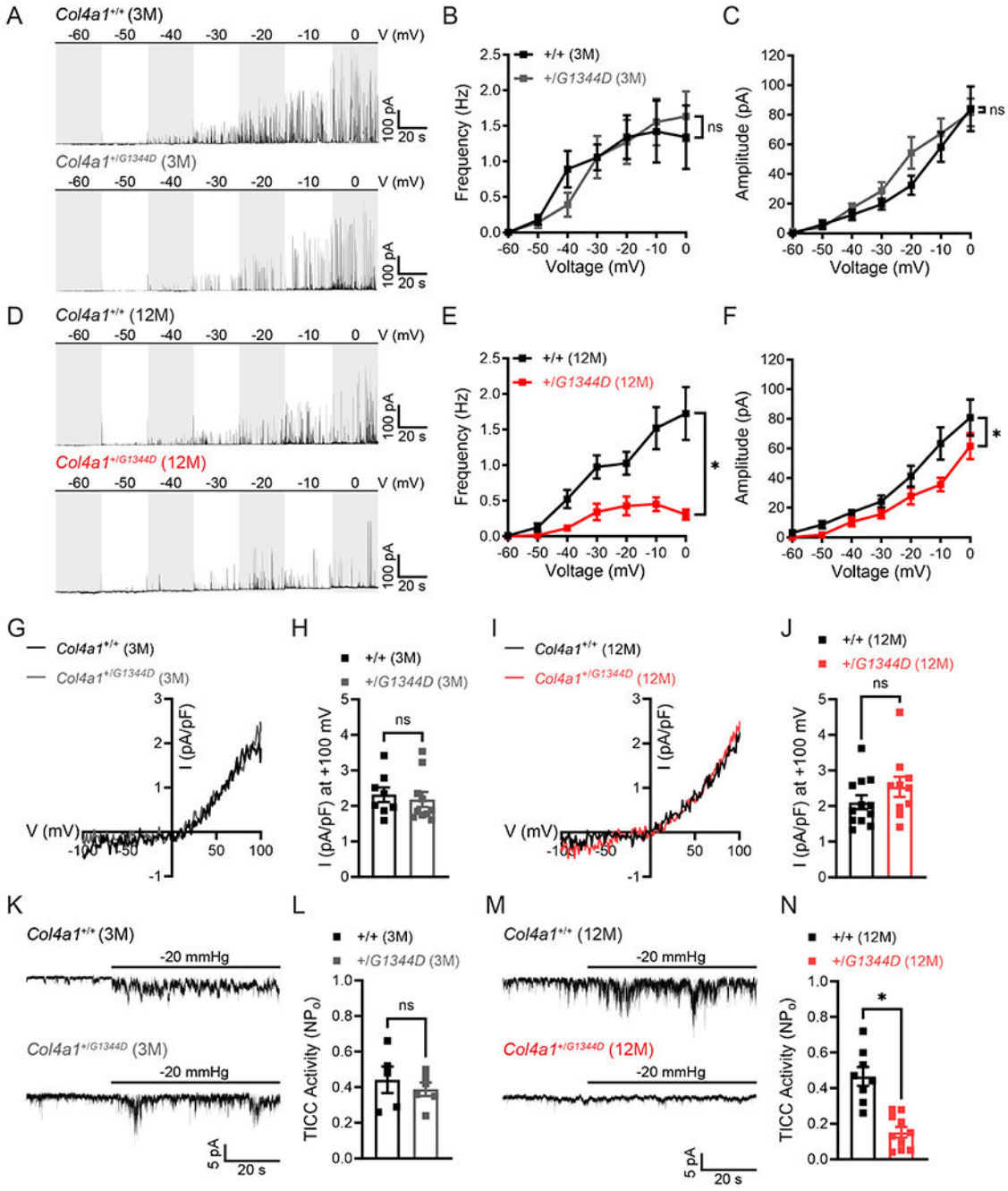

Figure 3. Age-dependent declines in BK and TRPM4 channel activity in SMCs from *Col4a1*$^{+/G1344D}$ mice.

(A) Representative traces of spontaneous transient outward currents (STOCs) in freshly isolated cerebral artery smooth muscle cells (SMCs) from 3 M-old *Col4a1*$^{+/+}$ and *Col4a1*$^{+/G1344D}$ mice over a range of membrane potentials (−60 to 0 mV). **(B and C)** Summary data showing STOC frequency (B) and amplitude (C) at each command potential. n = 8-12 cells from 5 animals per group. ns = not significant, two-way ANOVA. **(D)** Representative traces of STOCs in cerebral artery SMCs from 12 M-old *Col4a1*$^{+/+}$

and *Col4a1*$^{+/G1344D}$ mice. **(E and F)** Summary data showing STOC frequency (E) and amplitude (F) at each command potential. n = 12 cells from 5 animals per group. *P ≤ 0.05, two-way ANOVA. **(G)** Representative I-V plots of whole-cell patch-clamp TRPM4 current recordings during voltage ramps (−100 to 100 mV) in cerebral artery SMCs from 3 M-old *Col4a1*$^{+/+}$ and *Col4a1*$^{+/G1344D}$ mice. Currents were evoked by including 200 μM free Ca^{2+} in the intracellular solution, and the TRPM4 portion of the current was determined by adding the TRPM4 blocker 9-phenanthrol (30 μM). **(H)** Summary of whole-cell TRPM4 current density at +100 mV. n = 8-10 cells from 3 or 4 animals per group. ns = not significant, unpaired t-test. **(I)** Representative I-V plots of whole-cell patch-clamp TRPM4 current recordings in cerebral artery SMCs from 12 M-old *Col4a1*$^{+/+}$ and *Col4a1*$^{+/G1344D}$ mice. **(J)** Summary of whole-cell TRPM4 current density at +100 mV. n = 10-12 cells from 4 animals per group. ns = not significant, unpaired t-test. **(K)** Representative traces of transient inward cation currents (TICCs) evoked by applying negative pressure (−20 mmHg) to stretch the plasma membrane of voltage-clamped (−70 mV) cerebral artery SMCs isolated from 3 M-old *Col4a1*$^{+/+}$ and *Col4a1*$^{+/G1344D}$ mice. **(L)** Summary data of TICC activity. n = 5-6 cells from 3 animals per group. ns = not significant, unpaired t-test. **(M)** Representative traces of TICCs in cerebral artery SMCs isolated from 12 M-old *Col4a1*$^{+/+}$ and *Col4a1*$^{+/G1344D}$ mice. **(N)** Summary data of TICC activity. n = 8-10 cells from 4 or 5 animals per group. *P ≤ 0.05, unpaired t-test.

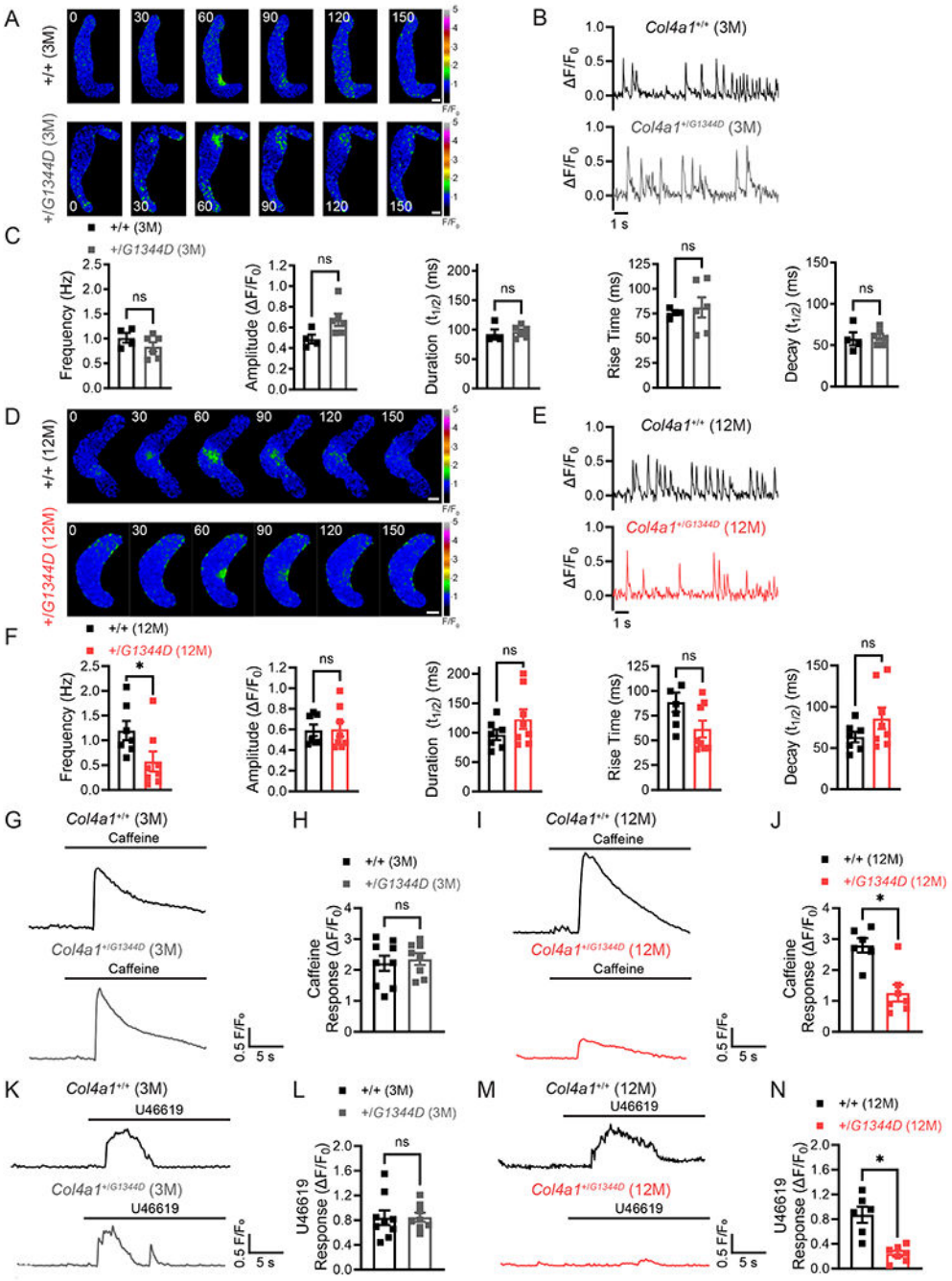

Figure 4. Defective intracellular Ca^{2+} signaling in cerebral artery SMCs from 12 M-old *Col4a1*$^{+/G1344D}$ mice.

(A) Representative time-course spinning disk confocal images exhibiting Ca^{2+} spark events in Fluo-4-AM loaded cerebral artery smooth muscle cells (SMCs) from 3 M-old *Col4a1*$^{+/+}$ and *Col4a1*$^{+/G1344D}$ mice. Time = milliseconds, scale bar = 5 μm. **(B)** Representative traces of Ca^{2+} spark events in cerebral artery SMCs isolated from 3 M-old *Col4a1*$^{+/+}$ and *Col4a1*$^{+/G1344D}$ mice presented as changes in fractional fluorescence ($\Delta F/F_0$) over time. **(C)** Summary data showing Ca^{2+} spark frequency, amplitude, duration, rise time, and decay. n =

4-6 cells from 3 animals per group. ns = not significant, unpaired t-test. **(D)** Representative time-course images exhibiting Ca^{2+} spark events in cerebral artery SMCs from 12 M-old *Col4a1*$^{+/+}$ and *Col4a1*$^{+/G1344D}$. Time = milliseconds, scale bar = 5 μm. **(E)** Representative traces of Ca^{2+} spark events in cerebral artery SMCs isolated from 12 M-old *Col4a1*$^{+/+}$ and *Col4a1*$^{+/G1344D}$ mice presented as $\Delta F/F_0$ over time. **(F)** Summary data showing Ca^{2+} spark frequency, amplitude, duration, rise time, and decay. n = 7-8 cells from 3 or 4 animals per group. *P ≤ 0.05, ns = not significant, unpaired t-test. **(G)** Representative traces showing whole-cell F/F_0 changes in response to caffeine (10 mM) in Fluo-4-AM loaded cerebral artery SMCs from 3 M-old *Col4a1*$^{+/+}$ and *Col4a1*$^{+/G1344D}$ mice. **(H)** Summary data of the $\Delta F/F_0$ in response to caffeine. n = 8-9 cells from 3 animals per group. ns = not significant, unpaired t-test. **(I)** Representative traces showing whole-cell F/F_0 changes in response to caffeine in SMCs from 12 M-old *Col4a1*$^{+/+}$ and *Col4a1*$^{+/G1344D}$ mice. **(J)** Summary data of the $\Delta F/F_0$ in response to caffeine. n = 6-7 cells from 3 animals per group. *P ≤ 0.05, unpaired t-test. **(K)** Representative traces showing whole-cell F/F_0 changes in response to U46619 (100 nM) in Fluo-4-AM loaded cerebral artery SMCs from 3 M-old *Col4a1*$^{+/+}$ and *Col4a1*$^{+/G1344D}$ mice. **(L)** Summary data of the $\Delta F/F_0$ in response to U46619. n = 8-9 cells from 3 animals per group. ns = not significant, unpaired t-test. **(M)** Representative traces showing whole-cell F/F_0 changes in response to U46619 in SMCs from 12 M-old *Col4a1*$^{+/+}$ and *Col4a1*$^{+/G1344D}$ mice. **(N)** Summary data of the $\Delta F/F_0$ in response to U46619. n = 6-7 cells from 3 animals per group. *P ≤ 0.05, unpaired t-test.

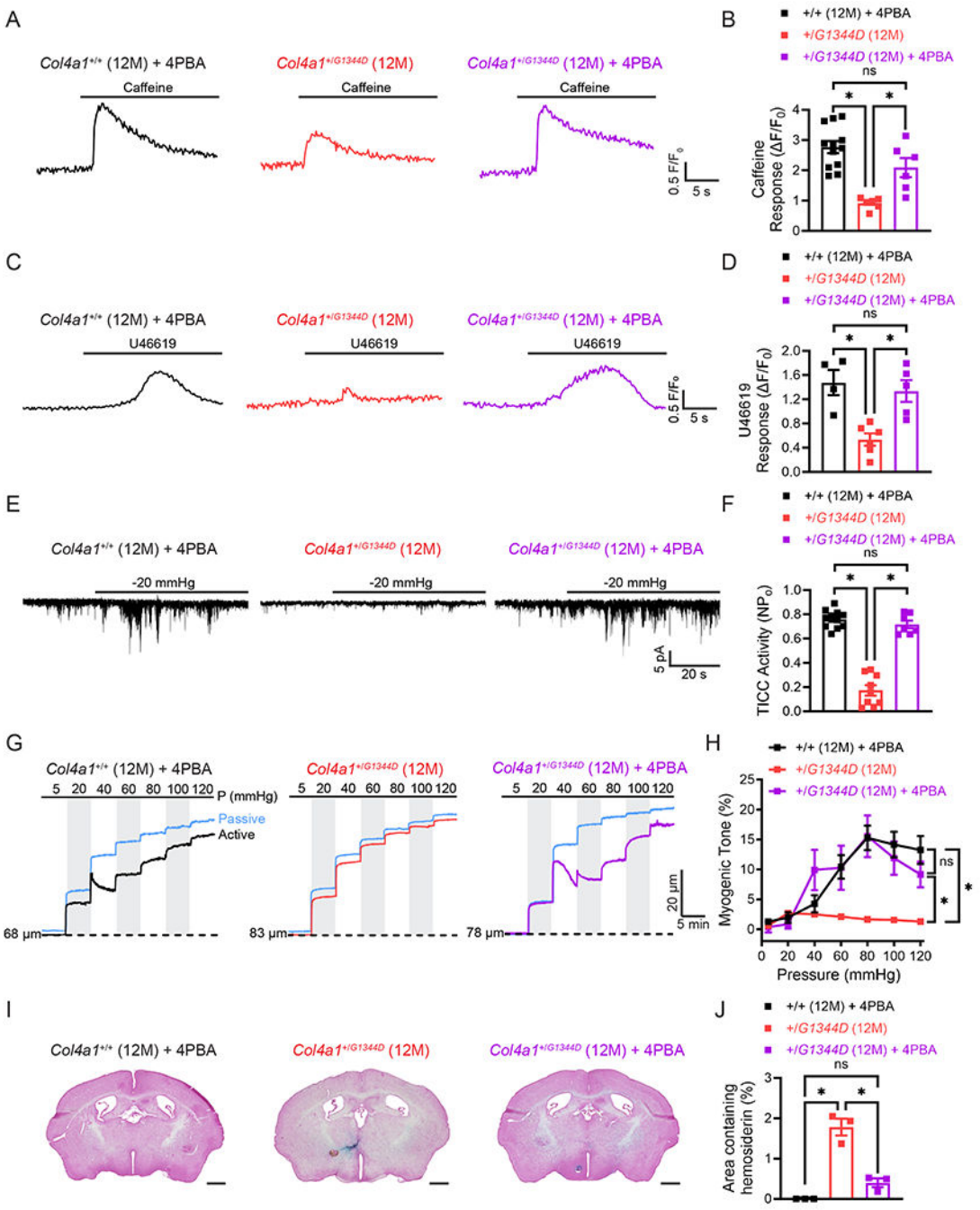

Figure 5. 4PBA prevents age-related cerebral artery defects in *Col4a1*$^{+/G1344D}$ mice.

(A) Representative traces showing whole-cell F/F_0 changes in response to caffeine (10 mM) in Fluo-4-AM loaded cerebral artery SMCs from 4PBA treated 12 M-old *Col4a1*$^{+/+}$ and *Col4a1*$^{+/G1344D}$ and untreated *Col4a1*$^{+/G1344D}$ mice. **(B)** Summary data of $\Delta F/F_0$ in response to caffeine. n = 6-12 cells from 3-4 animals per group. *P ≤ 0.05, ns = not significant, one-way ANOVA followed by Tukey's multiple comparisons post-hoc test. **(C)** Representative traces showing whole-cell F/F_0 changes in response to U46619 (100 nM) in Fluo-4-AM loaded cerebral artery SMCs from 4PBA treated 12 M-old *Col4a1*$^{+/+}$ and

Col4a1$^{+/G1344D}$ and untreated *Col4a1*$^{+/G1344D}$ mice. **(D)** Summary data of $\Delta F/F_0$ in response to U46619. n = 4-6 cells from 3-4 animals per group. *P ≤ 0.05, ns = not significant, one-way ANOVA followed by Tukey's multiple comparisons post-hoc test. **(E)** Representative traces of transient inward cation currents (TICCs) evoked by applying negative pressure (−20 mmHg) to stretch the plasma membrane of voltage-clamped (−70 mV) cerebral artery SMCs isolated from 4PBA treated 12 M-old *Col4a1*$^{+/+}$ and *Col4a1*$^{+/G1344D}$ and untreated *Col4a1*$^{+/G1344D}$ mice. **(F)** Summary data of TICC activity. n = 7-11 cells from 3-4 animals per group. *P ≤ 0.05, ns = not significant, one-way ANOVA followed by Tukey's multiple comparisons post-hoc test. **(G)** Representative recordings of the inner diameter of isolated cerebral arteries from 4PBA-treated 12 M-old *Col4a1*$^{+/+}$ and *Col4a1*$^{+/G1344D}$ and untreated *Col4a1*$^{+/G1344D}$ mice showing the myogenic response to increases in pressure (active) and the dilation of the same arteries when extracellular Ca^{2+} has been removed (passive). **(H)** Summary data of myogenic tone as a function of intraluminal pressure. n = 6 or 9 vessels from 3 or 5 mice. *P ≤ 0.05, ns = not significant, two-way ANOVA followed by Sidak's multiple comparisons post-hoc test. **(I)** Representative images of Prussian blue stained brain sections from 4PBA treated 12 M-old *Col4a1*$^{+/+}$ and *Col4a1*$^{+/G1344D}$ and untreated *Col4a1*$^{+/G1344D}$ mice. Scale bar = 1 mm. **(J)** Summary data presented as percentage of brain area with Prussian blue staining in brain sections (500 μm intervals). N = 3 animals per group. *P ≤ 0.05, ns = not significant, one-way ANOVA followed by Tukey's multiple comparisons post-hoc test.

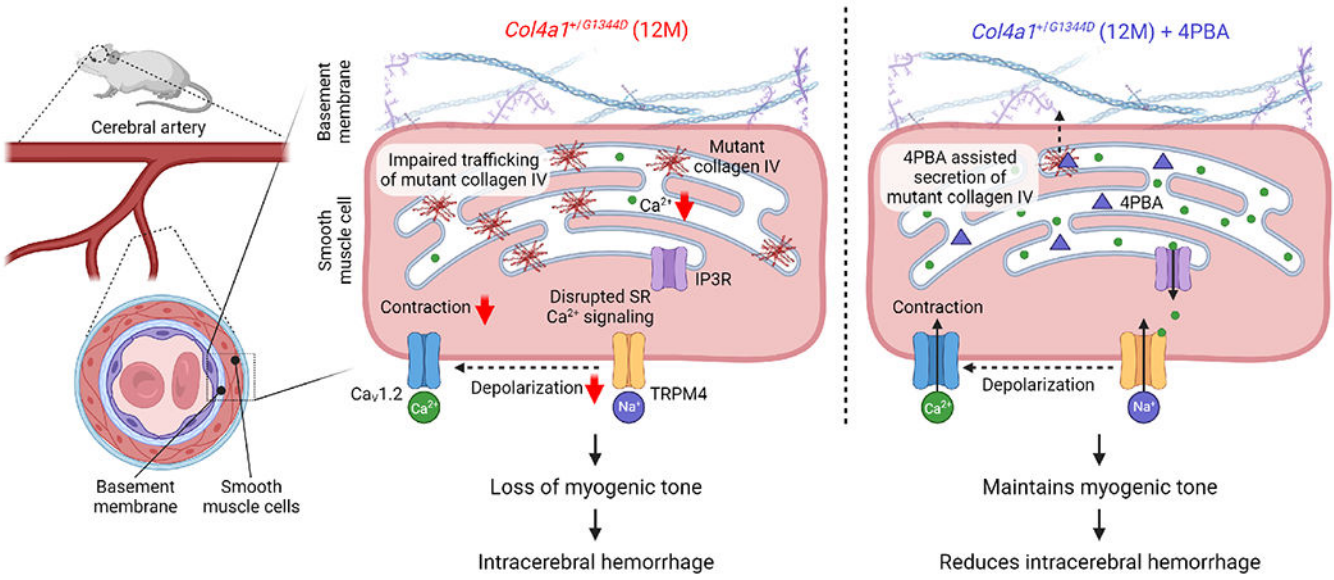

Figure 6. Proposed mechanism for *Col4a1*^{G1344D}-linked cSVD.

Impaired trafficking of mutant collagen IV in the sarcoplasmic reticulum (SR) of cerebral artery smooth muscle cells (SMCs) causes a decrease in SR Ca^{2+}. Reduction of SR Ca^{2+} disrupts Ca^{2+} signaling between inositol trisphosphate receptors (IP_3Rs) and transient receptor potential melastatin 4 (TRPM4) channels. Decreased TRPM4 channel activity impairs pressure-induced depolarization and decreases voltage-dependent Ca^{2+} influx through $Ca_V1.2$ Ca^{2+} channels causing a decrease in SMC contractility. Impaired cerebral artery SMC contraction causes a loss of myogenic tone that increases susceptibility to intracerebral hemorrhage. Treating mice with 4-phenylbutyrate (4PBA), a small molecule with chaperone properties, promotes the secretion of mutant collagen IV, thereby preventing reduction of SR Ca^{2+} and associated downstream defects.